Supporting Information for "MCADAM: A continuous paleomagnetic dipole moment model for at least 3.7 billion years"

Richard K. Bono[1], Greig A. Paterson[2], and Andrew J. Biggin[2]

[1]Department of Earth, Ocean and Atmospheric Science, Florida State University, FL 32304, USA

[2]Department of Earth, Ocean and Ecological Sciences, University of Liverpool, Liverpool L697ZE, UK

Contents of this file

1. Text S1

2. Figures S1 to S5

3. Table S1

Additional Supporting Information (Files uploaded separately)

1. PINT v8.1.0 database. Available at `http://www.pintdb.org`, see website or Bono et al. (2022) for complete description.

2. MCADAM.1a – MCADAM.1c. Available at `http://www.earthref.org/ERDA/2537/`.

―――――

Corresponding author: Richard K. Bono, Department of Earth, Ocean and Atmospheric Science, Florida State University, FL, USA (rbono@fsu.edu)

`August 30, 2022, 8:03pm`

Columns:

(i) `0..N` : Time step index

(ii) `age` : Age step realization (Ma)

(iii) `mean` : MCADAM mean dipole (1e22 Am^2)

(iv) `std` : MCADAM dipole standard deviation (1e22 Am^2)

(v) `mode` : MCADAM dipole mode (1e22 Am^2)

(vi) `2.5%` : MCADAM dipole 2.5% percentile (1e22 Am^2)

(vii) `25%` : MCADAM dipole 25% percentile (1e22 Am^2)

(viii) `50%` : MCADAM dipole 50% percentile (1e22 Am^2)

(ix) `75%` : MCADAM dipole 75% percentile (1e22 Am^2)

(x) `97.5%` : MCADAM dipole 97.5% percentile (1e22 Am^2)

Text S1. MCADAM sensitivity testing

To test the ability for the MCADAM modeling approach to recover true temporal variation of the average paleomagnetic field, we conducted a series of synthetic tests exploring models sensitivity to sampling density and distribution, as well as the data uncertainty in site mean age and dipole moment. We first define a "true" time-varying dipole field, here a combination of sine waves with the variation of PADM2M (Ziegler et al., 2011) superimposed over the baselines signal. Site mean age distributions are defined to mimic the PINT v8.1.0 distribution of ages. Synthetic paleointensity samples are realized from this "true" mean trend using a Gaussian distribution with a mean corresponding to the mean field predicted by the true dipole moment and a σ inferred from PINT v8.1.0, this variation represents a combination of secular variation and measurement noise, and Gaussian draw for the site age with increasing age uncertainty from 100 kyr to 20 Myr depending on site age (< 1 Myr and > 1 Gyr, respectively). While the "true" mean field does not resemble the paleomagnetic field, and the variation is arbitrarily defined, visually this synthetic field record appears to share broadly similar features to the paleomagnetic record in the PINT v8.1.0 database such that we feel it represents a reasonably synthetic analogue for sensitivity testing. The MCADAM modelling approach is applied to this synthetic dataset, using the synthetic VDM realizations to estimate the mean dipole field strength.

The results of these sensitivity tests demonstrate that generally the modeling approach is capable of reproducing the "true" median field temporal trend within the 75-95% interval of time trends. The MCADAM-derived model was able to estimate the true field

August 30, 2022, 8:03pm

strength within the 95% predictive interval over 99% of the time, within the 75% predictive interval over 80% of the time, and yields a root-mean-square misfit of 1.7 ZAm^2. Visually, the MCADAM model's predictive interval reacts appropriately for the data density and distribution, with the predictive interval shrinking when the density of observations is high and enlarging when the density is low or the scatter is high.

References

Abdulghafur, F., & Bowles, J. A. (2019). Absolute Paleointensity Study of Miocene Tiva Canyon Tuff, Yucca Mountain, Nevada: Role of Fine-Particle Grain-Size Variations. *Geochemistry, Geophysics, Geosystems*, *20*(12), 5818–5830. doi: 10.1029/2019GC008728

Asefaw, H., Tauxe, L., Koppers, A. a. P., & Staudigel, H. (2021). Four-Dimensional Paleomagnetic Dataset: Plio-Pleistocene Paleodirection and Paleointensity Results From the Erebus Volcanic Province, Antarctica. *Journal of Geophysical Research: Solid Earth*, *126*(2), e2020JB020834. doi: 10.1029/2020JB020834

Biggin, A. J., Piispa, E. J., Pesonen, L. J., Holme, R., Paterson, G. A., Veikkolainen, T., & Tauxe, L. (2015). Palaeomagnetic field intensity variations suggest Mesoproterozoic inner-core nucleation. *Nature*, *526*(7572), 245–248. doi: 10.1038/nature15523

Bono, R. K., Paterson, G. A., van der Boon, A., Engbers, Y. A., Michael Grappone, J., Handford, B., ... Biggin, A. J. (2022). The PINT database: A definitive compilation of absolute palaeomagnetic intensity determinations since 4 billion years ago. *Geophysical Journal International*, *229*(1), 522–545. doi: 10.1093/gji/ggab490

Bono, R. K., Tarduno, J. A., Nimmo, F., & Cottrell, R. D. (2019). Young inner core inferred from Ediacaran ultra-low geomagnetic field intensity. *Nature Geoscience*, *12*(2), 143–147. doi: 10.1038/s41561-018-0288-0

Calvo-Rathert, M., Bógalo, M. F., Morales, J., Goguitchaichvili, A., Lebedev, V. A., Vashakidze, G., ... Herrero-Bervera, E. (2021). An Integrated Paleomagnetic, Multimethod-Paleointensity, and Radiometric Study on Cretaceous and Paleogene

Lavas From the Lesser Caucasus: Geomagnetic and Tectonic Implications. *Journal of Geophysical Research: Solid Earth*, *126*(2), e2020JB020019. doi: 10.1029/2020JB020019

Cervantes-Solano, M., Goguitchaichvili, A., Sánchez Bettucci, L., Morales-Contreras, J., Gogorza, C., & Núñez, P. (2020). An integrated paleomagnetic and multispecimen paleointensity study from the late Jurassic Zapicán dike swarm (Uruguay). *Journal of South American Earth Sciences*, *104*, 102815. doi: 10.1016/j.jsames.2020.102815

Chang, B., Kim, W., Doh, S.-J., & Yu, Y. (2013). Paleointensity determination of Late Cretaceous basalts in northwest South Korea: Implications for low and stable paleofield strength in the Late Cretaceous. *Earth, Planets and Space*, *65*(12), 1501–1513. doi: 10.5047/eps.2013.09.013

Chauvin, A., Roperch, P., & Levi, S. (2005). Reliability of geomagnetic paleointensity data: The effects of the NRM fraction and concave-up behavior on paleointensity determinations by the Thellier method. *Physics of the Earth and Planetary Interiors*, *150*(4), 265–286. doi: 10.1016/j.pepi.2004.11.008

Døssing, A., Muxworthy, A. R., Supakulopas, R., Riishuus, M. S., & Mac Niocaill, C. (2016). High northern geomagnetic field behavior and new constraints on the Gilsá event: Paleomagnetic and 40Ar/39Ar results of ∼0.5–3.1 Ma basalts from Jökuldalur, Iceland. *Earth and Planetary Science Letters*, *456*, 98–111. doi: 10.1016/j.epsl.2016.09.022

Eitel, M., Gilder, S. A., Spray, J., Thompson, L., & Pohl, J. (2016). A paleomagnetic and rock magnetic study of the Manicouagan impact structure: Implications for crater

formation and geodynamo effects. *Journal of Geophysical Research: Solid Earth*, *121*(2), 436–454. doi: 10.1002/2015JB012577

Eliseev, A., Shcherbakova, V., Metelkin, D., Mikhaltsov, N., Zhidkov, G., Abashev, V., & Rogov, A. (2021). Low Geomagnetic Field Paleointensity on the Permian–Triassic Boundary from Study of the Kuznetsk Basin Traps (Southern Siberia). *Russian Geology and Geophysics*. doi: 10.2113/RGG20204330

Engbers, Y. A., Grappone, J. M., Mark, D. F., & Biggin, A. J. (2022). Low Paleointensities and Ar/Ar Ages From Saint Helena Provide Evidence for Recurring Magnetic Field Weaknesses in the South Atlantic. *Journal of Geophysical Research: Solid Earth*, *127*(3), e2021JB023358. doi: 10.1029/2021JB023358

Goguitchaichvili, A., Alva-Valdivia, L. M., Urrutia-Fucugauchi, J., Morales, J., & Ferrari, L. (2000). Absolute palaeointensity results from the Trans-Mexican Volcanic Belt: Implications for the late Miocene geomagnetic field strength. *Geophysical Journal International*, *143*, 977–984. doi: 10.1046/j.1365-246X.2000.01301.x

Hawkins, L. M. A., Grappone, J. M., Sprain, C. J., Saengduean, P., Sage, E. J., Thomas-Cunningham, S., ... Biggin, A. J. (2021). Intensity of the Earth's magnetic field: Evidence for a Mid-Paleozoic dipole low. *Proceedings of the National Academy of Sciences*, *118*(34). doi: 10.1073/pnas.2017342118

Kapawar, M. R., & Mamilla, V. (2021). Paleointensity of the Earth's magnetic field at ∼117 Ma determined from the Rajmahal and Sylhet Trap Basalts, India. *Journal of Earth System Science*, *130*(3), 154. doi: 10.1007/s12040-021-01652-9

Kulakov, E., Sprain, C., Doubrovine, P., Smirnov, A., Paterson, G., Hawkins, L., ...

Biggin, A. (2019). Analysis of an updated paleointensity database (Q $_{PI}$ -PINT) for 65-200 Ma: Implications for the long-term history of dipole moment through the Mesozoic. *Journal of Geophysical Research: Solid Earth*, 2018JB017287. doi: 10.1029/2018JB017287

Lloyd, S. J., Biggin, A. J., Halls, H., & Hill, M. J. (2021). First palaeointensity data from the cryogenian and their potential implications for inner core nucleation age. *Geophysical Journal International*, *226*(1), 66–77. doi: 10.1093/gji/ggab090

Lloyd, S. J., Biggin, A. J., & Li, Z.-X. (2021). New Paleointensity Data Suggest Possible Phanerozoic-Type Paleomagnetic Variations in the Precambrian. *Geochemistry, Geophysics, Geosystems*, *22*(10). doi: 10.1029/2021GC009990

Lloyd, S. J., Biggin, A. J., Paterson, G. A., & McCausland, P. J. A. (2022). Extremely weak early Cambrian dipole moment similar to Ediacaran: Evidence for long-term trends in geomagnetic field behaviour? *Earth and Planetary Science Letters*, *595*, 117757. doi: 10.1016/j.epsl.2022.117757

Mahgoub, A. N., García-Amador, B. I., & Alva-Valdivia, L. M. (2021). Comprehensive palaeomagnetic study of San Borja and Jaraguay monogenetic volcanic fields, Baja California (28–30°N): Considerations on latitudinal corrections. *Geophysical Journal International*, *225*(3), 1897–1919. doi: 10.1093/gji/ggab064

Meng, J., Lhuillier, F., Wang, C., Liu, H., Eid, B., & Li, Y. (2020). Paleomagnetism of Paleocene-Maastrichtian (60–70 Ma) Lava Flows From Tian Shan (Central Asia): Directional Analysis and Paleointensities. *Journal of Geophysical Research: Solid Earth*, *125*(9). doi: 10.1029/2019JB018631

August 30, 2022, 8:03pm

Miki, M., Seki, H., Yamamoto, Y., Gouzu, C., Hyodo, H., Uno, K., & Otofuji, Y.-i. (2020). Paleomagnetism, paleointensity and geochronology of a Proterozoic dolerite dyke from southern West Greenland. *Journal of Geodynamics*, *139*, 101752. doi: 10.1016/j.jog.2020.101752

Radhakrishna, T., Asanulla, M. R., Venkateshwarlu, M., & Soumya, G. S. (2020). Low geomagnetic field strength during End-Cretaceous Deccan volcanism and whole mantle convection. *Scientific Reports*, *10*(1), 10743. doi: 10.1038/s41598-020-67245-6

Rosenqvist, L., Opgenoorth, H., Buchert, S., McCrea, I., Amm, O., & Lathuillere, C. (2005). Extreme solar-terrestrial events of October 2003: High-latitude and Cluster observations of the large geomagnetic disturbances on 30 October. *Journal of Geophysical Research: Space Physics*, *110*(A9). doi: 10.1029/2004JA010927

Sánchez-Moreno, E. M., Calvo-Rathert, M., Goguitchaichvili, A., Tauxe, L., Vashakidze, G. T., & Lebedev, V. A. (2020). Weak palaeointensity results over a Pliocene volcanic sequence from Lesser Caucasus (Georgia): Transitional record or time averaged field? *Geophysical Journal International*, *220*(3), 1604–1618. doi: 10.1093/gji/ggz533

Sánchez-Moreno, E. M., Calvo-Rathert, M., Goguitchaichvili, A., Vashakidze, G. T., Camps, P., Morales-Contreras, J., . . . Lebedev, V. A. (2021). Paleointensity Results From Pliocene Lavas of the Lesser Caucasus Obtained Using the Multispecimen Parallel Differential pTRM Method: A Comparison With Thellier-Thellier and IZZI Data. *Journal of Geophysical Research: Solid Earth*, *126*(4), e2020JB019682. doi: 10.1029/2020JB019682

Schnepp, E., Arneitz, P., Ganerød, M., Scholger, R., Fritz, I., Egli, R., & Leonhardt, R.

(2021). Intermediate field directions recorded in Pliocene basalts in Styria (Austria): Evidence for cryptochron C2r.2r-1. *Earth, Planets and Space*, *73*(1), 182. doi: 10.1186/s40623-021-01518-w

Shcherbakova, V. V., Bakhmutov, V. G., Thallner, D., Shcherbakov, V. P., Zhidkov, G. V., & Biggin, A. J. (2020). Ultra-low palaeointensities from East European Craton, Ukraine support a globally anomalous palaeomagnetic field in the Ediacaran. *Geophysical Journal International*, *220*(3), 1928–1946. doi: 10.1093/gji/ggz566

Tarduno, J. A., Cottrell, R. D., Bono, R. K., Oda, H., Davis, W. J., Fayek, M., . . . Blackman, E. G. (2020). Paleomagnetism indicates that primary magnetite in zircon records a strong Hadean geodynamo. *Proceedings of the National Academy of Sciences*, *117*(5), 2309–2318. doi: 10.1073/pnas.1916553117

Thallner, D., Biggin, A. J., & Halls, H. C. (2021). An extended period of extremely weak geomagnetic field suggested by palaeointensities from the Ediacaran Grenville dykes (SE Canada). *Earth and Planetary Science Letters*, *568*, 117025. doi: 10.1016/j.epsl.2021.117025

Thallner, D., Biggin, A. J., McCausland, P. J. A., & Fu, R. R. (2021). New Paleointensities From the Skinner Cove Formation, Newfoundland, Suggest a Changing State of the Geomagnetic Field at the Ediacaran-Cambrian Transition. *Journal of Geophysical Research: Solid Earth*, *126*(9). doi: 10.1029/2021JB022292

Thallner, D., Shcherbakova, V. V., Bakhmutov, V. G., Shcherbakov, V. P., Zhidkov, G. V., Poliachenko, I. B., & Biggin, A. J. (2022). New palaeodirections and palaeointensity data from extensive profiles through the Ediacaran section of the Volyn Basalt

Province (NW Ukraine). *Geophysical Journal International*, *231*(1), 474–492. doi: 10.1093/gji/ggac186

Yoshimura, Y., Yamazaki, T., Yamamoto, Y., Ahn, H.-S., Kidane, T., & Otofuji, Y.-i. (2020). Geomagnetic Paleointensity Around 30 Ma Estimated From Afro-Arabian Large Igneous Province. *Geochemistry, Geophysics, Geosystems*, *21*(12). doi: 10.1029/2020GC009341

Zhang, Y., Swanson-Hysell, N. L., Avery, M. S., & Fu, R. R. (2022, July). High geomagnetic field intensity recorded by anorthosite xenoliths requires a strongly powered late Mesoproterozoic geodynamo. *Proceedings of the National Academy of Sciences of the United States of America*, *119*(29), e2202875119. doi: 10.1073/pnas.2202875119

Zhou, T., Tarduno, J. A., Nimmo, F., Cottrell, R. D., Bono, R. K., Ibanez-Mejia, M., . . . Padgett, F. (2022, July). Early Cambrian renewal of the geodynamo and the origin of inner core structure. *Nature Communications*, *13*(1), 4161. doi: 10.1038/s41467-022-31677-7

Ziegler, L. B., Constable, C. G., Johnson, C. L., & Tauxe, L. (2011). PADM2M: A penalized maximum likelihood model of the 0–2 Ma palaeomagnetic axial dipole moment. *Geophysical Journal International*, *184*(3), 1069–1089. doi: 10.1111/j.1365-246X.2010.04905.x
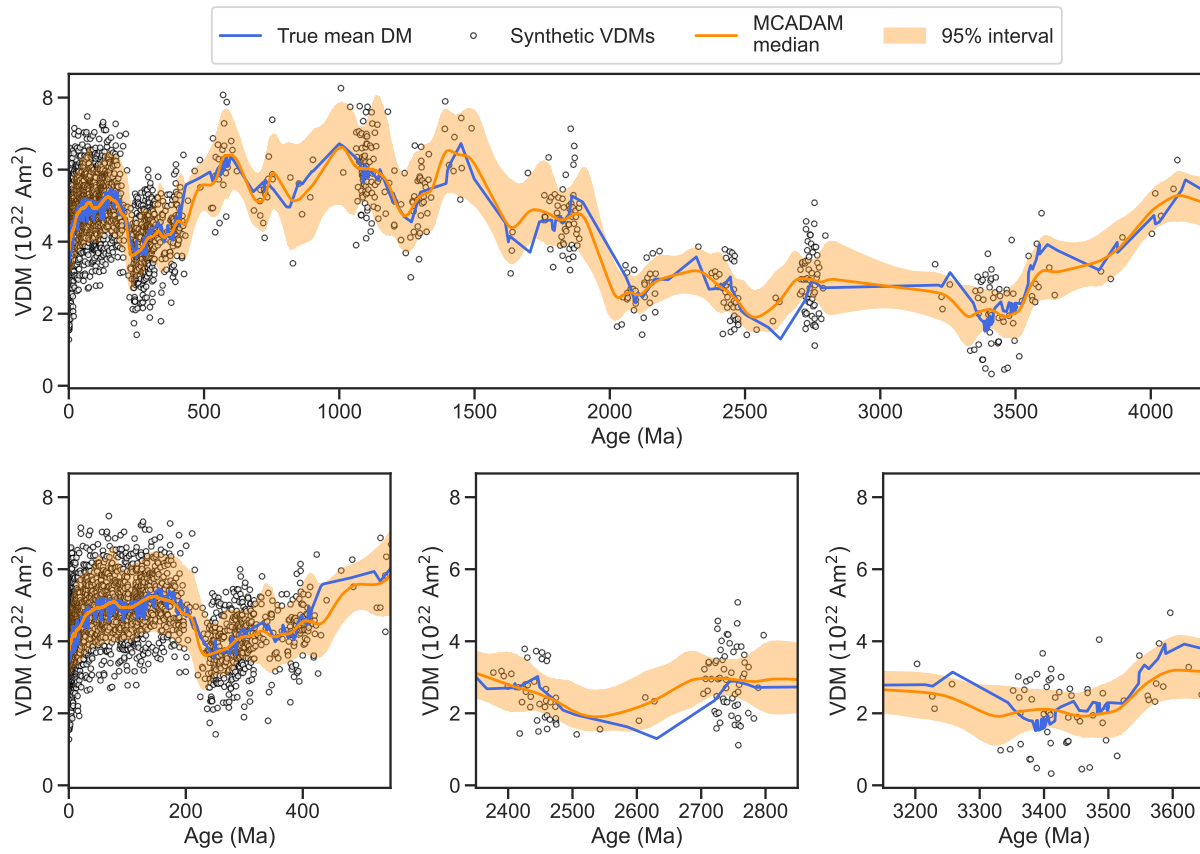
Figure S1.   Synthetic test of MCADAM using a known dipole mean field with realistic variation. Blue line: true mean dipole moment; grey circles: synthetic VDMs drawn from true mean dipole moment with plausible variance; orange line and field, MCADAM model median field strength estimate and 95% predictive interval.
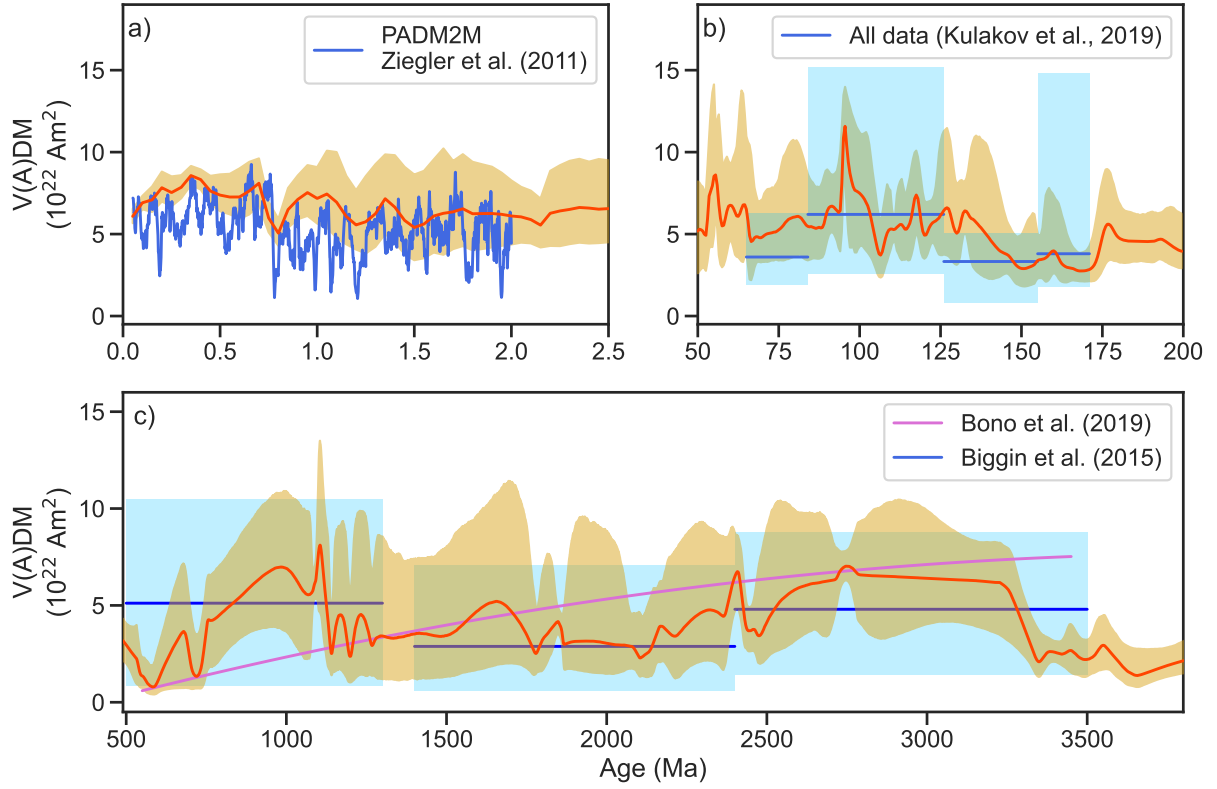
Figure S2.   MCADAM.1a time-varying model of paleofield strength for the past 3.7 billion years from all non-transitional sites in the PINT v8.1.0 database. In all panels, the orange line represents the median time-varying model from MCADAM.1b with shaded 95% interval. a) Quaternary; blue line shows PADM2M model (Ziegler et al., 2011); b) Mesozoic; blue line and field shows median and 95% interval of Q_{PI} binned following (Kulakov et al., 2019); c) Precambrian; purple line shows polynomial fit of Bono et al. (2019), blue lines show bin medians with shaded 95% confidence intervals of Biggin et al. (2015).

August 30, 2022, 8:03pm
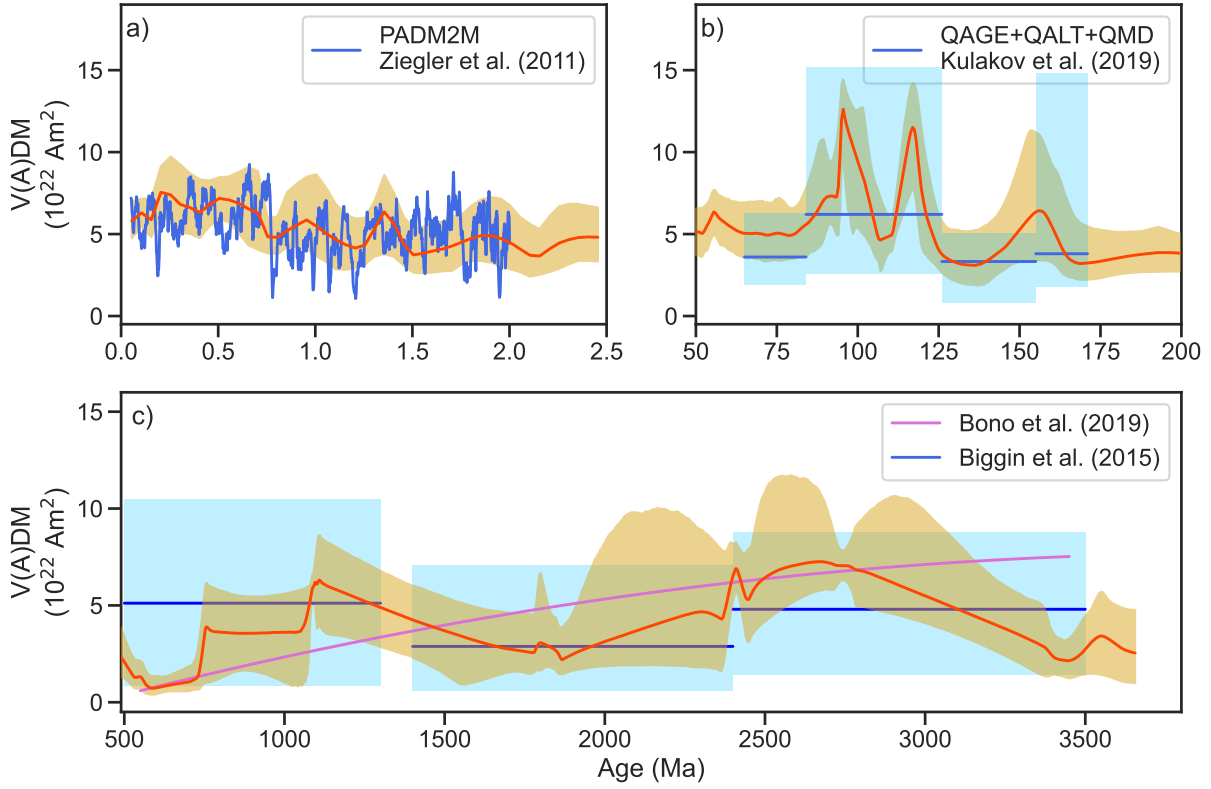
Figure S3.   MCADAM.1c time-varying model of paleofield strength for the past 3.7 billion years from PINT v8.1.0 data meeting the prioritized Q_{PI} criteria: QAGE + QALT + QMD. In all panels, the orange line represents the median time-varying model from MCADAM.1b with shaded 95% interval. a) Quaternary; blue line shows PADM2M model (Ziegler et al., 2011); b) Mesozoic; blue line and field shows median and 95% interval of Q_{PI} binned following (Kulakov et al., 2019); c) Precambrian; purple line shows polynomial fit of Bono et al. (2019), blue lines show bin medians with shaded 95% confidence intervals of Biggin et al. (2015).
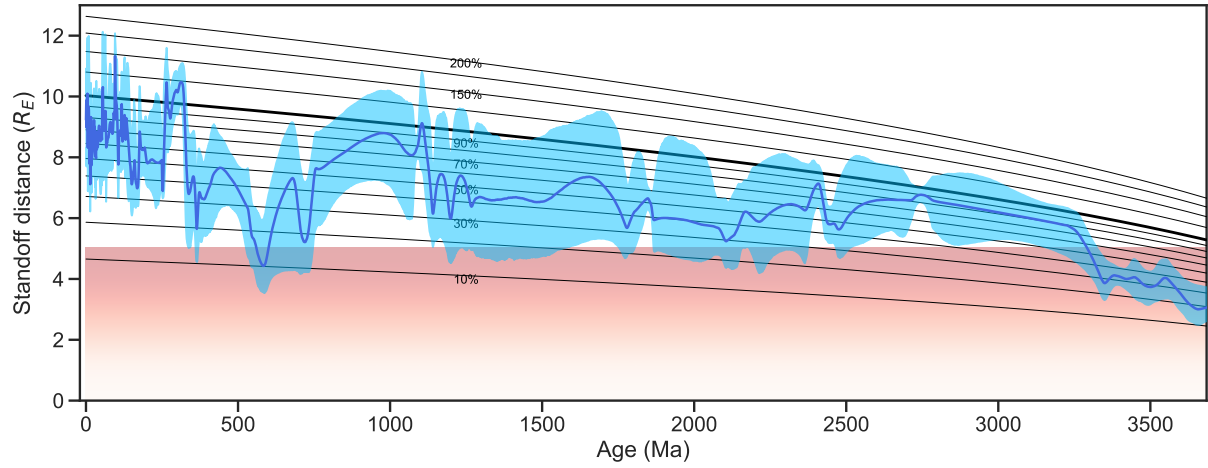
Figure S4. Magnetopause standoff distance estimate using equation 2 in the main text and the MCADAM.1a modeled dipole moment curve with from all non-transitional sites in the PINT v8.1.0 database. Blue curve is the predicted median dipole moment and blue field is the 95% predicted interval. Contour lines show standoff distance relative to the present day. Red gradient shows standoff distance associated with the Halloween 2003 solar storm (Rosenqvist et al., 2005).

Figure S5. Magnetopause standoff distance estimate using equation 2 in the main text and the MCADAM.1c modeled dipole moment curve with PINT v8.1.0 data meeting the prioritized Q_{PI} criteria: QAGE + QALT + QMD. Blue curve is the predicted median dipole moment and blue field is the 95% predicted interval. Contour lines show standoff distance relative to the present day. Red gradient shows standoff distance associated with the Halloween 2003 solar storm (Rosenqvist et al., 2005).
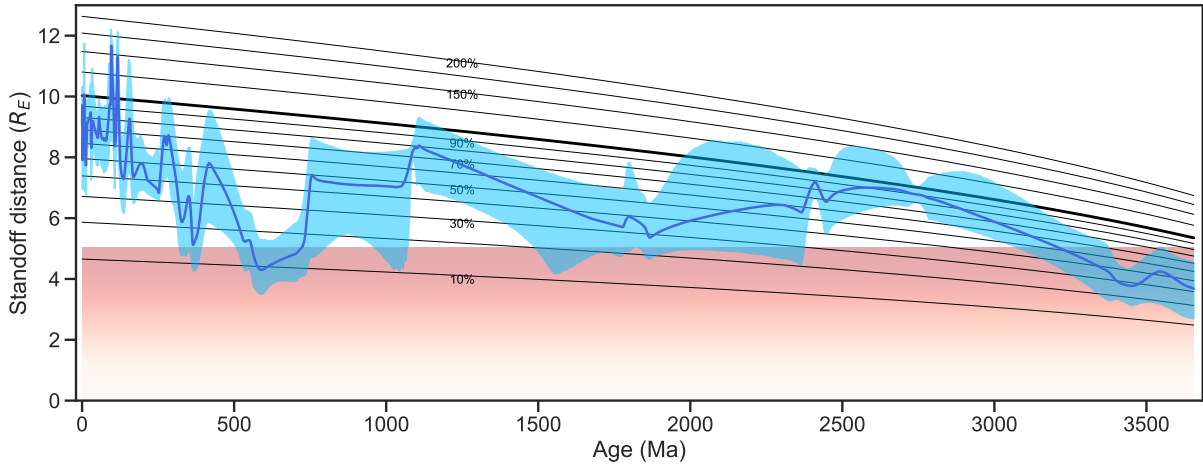
August 30, 2022, 8:03pm

Table S1.   New entries to PINT v8.1.0

REF	Site Lat.	Site Long.	Age	N_{Sites}	V(A)DM	Q_{PI}	Author (Year)
745	36.8	-116.5	12.7	2	6.09	6.0	Abdulghafur and Bowles (2019)
746	41.4	43.3	3.6	8	3.89	4.6	Sánchez-Moreno et al. (2020)
747	-33.5	-55.9	157.6	3	9.79	3.0	Cervantes-Solano et al. (2020)
749	64.4	-51.4	1818.0	1	2.33	6.0	Miki et al. (2020)
750	51.5	26.0	568.5	4	0.90	7.8	Shcherbakova et al. (2020)
751	-26.2	117.0	3495.5	24	1.88	2.1	Tarduno et al. (2020)
752	13.3	37.9	30.1	11	4.19	3.9	Yoshimura et al. (2020)
753	40.2	75.3	63.6	4	6.13	6.5	Meng et al. (2020)
754	17.3	73.7	65.5	10	1.18	3.0	Radhakrishna, Asanulla, Venkateshwarlu, and Soumya (2020)
755	-78.0	164.9	1.9	26	4.36	5.6	Asefaw, Tauxe, Koppers, and Staudigel (2021)
756	41.4	44.0	67.4	6	5.26	4.5	Calvo-Rathert et al. (2021)
757	56.3	-3.0	366.4	14	2.48	6.8	Hawkins et al. (2021)
758	25.1	88.7	117.0	10	3.50	1.0	Kapawar and Mamilla (2021)
759	76.4	-77.1	723.0	11	1.00	6.5	Lloyd, Biggin, Halls, and Hill (2021)
760	41.4	43.3	3.5	18	4.36	7.1	Sánchez-Moreno et al. (2021)
761	46.0	279.3	589.8	7	0.92	7.4	Thallner, Biggin, and Halls (2021)
762	-23.8	116.1	912.0	6	3.89	7.5	Lloyd, Biggin, and Li (2021)
763	54.8	87.1	250.0	4	1.72	5.5	Eliseev et al. (2021)
764	49.5	301.9	550.0	8	1.40	6.8	Thallner, Biggin, McCausland, and Fu (2021)
765	-15.9	-5.7	9.2	5	2.33	7.8	Engbers, Grappone, Mark, and Biggin (2022)
767	-16.8	208.6	2.6	2	7.34	4.0	Chauvin, Roperch, and Levi (2005)
768	41.5	43.3	3.8	6	6.89	1.0	Goguitchaichvili, Alva-Valdivia, Urrutia-Fucugauchi, Morales, and Ferrari (2000)
769	38.0	127.4	73.1	5	3.10	4.0	Chang, Kim, Doh, and Yu (2013)
770	65.1	-15.5	1.5	6	5.97	4.2	Døssing, Muxworthy, Supakulopas, Riishuus, and Mac Niocaill (2016)
772	51.5	-68.9	214.0	1	4.90	5.0	Eitel, Gilder, Spray, Thompson, and Pohl (2016)
774	29.1	-114.1	7.4	9	5.34	6.4	Mahgoub, García-Amador, and Alva-Valdivia (2021)
775	46.9	15.9	2.3	9	5.37	4.0	Schnepp et al. (2021)
777	42.7	268.9	1091.8	7	8.31	6.0	Zhang, Swanson-Hysell, Avery, and Fu (2022)
778	34.8	-98.9	532.5	1	3.50	6.0	Zhou et al. (2022)
779	45.7	-74.6	531.4	1	0.94	9.0	Lloyd, Biggin, Paterson, and McCausland (2022)
780	51.7	24.7	571.0	17	0.81	6.8	Thallner et al. (2022)

REF: study reference number in PINT v8.1.0; mean site location, Lat., Long. in degrees; mean site age in Ma; N_{Sites}: number of sites associated with the study; mean V(A)DM: virtual (axial) dipole moment, in 10^{22} Am^2; Q_{PI}: mean Q_{PI} score of sites associated with the study.